



Thermoelastic Analysis of Multilayered FG Spherical Shells Based on Lord–Shulman Theory

Yasin Heydarpour¹ · Parviz Malekzadeh¹

Received: 19 March 2018 / Accepted: 21 May 2018 / Published online: 26 May 2018
© Shiraz University 2018

Abstract

The thermoelastic wave in multilayered spherical shells with functionally graded (FG) layers under thermal boundary conditions is studied. The Lord–Shulman generalized coupled thermoelasticity theory is applied to illustrate the effect of finite heat wave speed. The material properties are assumed to be temperature dependent, and consequently, the governing equations become nonlinear ones. The layerwise-differential quadrature method together with Newmark time integration scheme and Newton–Raphson method are employed to solve the governing equations. The fast rate of convergence of the method is illustrated, and its accuracy is assessed by comparing the results with various existing solutions in the open literature wherever possible. Afterward, the effects of different parameters and also the temperature dependence of material properties on the transient thermoelastic responses of the FG spherical shells are studied and discussed. It is found that the temperature dependence of material properties, thermo-mechanical coupling, thickness-to-outer radius ratio and FG layer layout significantly affect the thermo-mechanical behavior of the FG shells.

Keywords Transient thermoelasticity · Functionally graded materials · Layered spherical shells · L–S theory · Layerwise-differential quadrature method

1 Introduction

Hollow spherical shells as important pressure vessels have found extensive applications in various modern industries such as aerospace, petroleum and nuclear engineering. In most cases, these structures should operate in high-temperature chemical environments. Hence, they should be protected for chemical and physical interaction of their materials with environments (i.e., corrosion and erosion) and also maintain their structural integrity under thermal conditions. In order to obtain such a desired performance, functionally graded materials (FGMs) as a new class of materials have been used to fabricate these types of pressure vessels (Obata and Noda 1994; Eslami et al. 2005; Shen 2009). The advantage of these advanced materials over the conventional laminated composite materials is that their physical properties vary smoothly and continuously in

spatial domain from one material to another one by suitable distribution of component materials, particularly along the thickness direction. Consequently, the disadvantageous problems of other composite types such as stress concentration phenomenon are reduced or eliminated. Usually, FGMs are made from a mixture of ceramic and metal. Ceramic constituents of FGMs are able to withstand high-temperature environments due to their favorable heat and corrosion resistance, while metal constituents have high tensile strength, toughness and bonding capability that provide stronger mechanical performance and reduce the possibility of catastrophic fracture.

In most previously studied thermoelasticity problems, the uncoupled classical thermoelasticity theory has been employed to investigate the thermoelastic behavior of the FG structural elements and the temperature distributions in the bodies have been estimated based on the Fourier heat conduction law; see, for example, Refs. (Ootao and Tanigawa 2004; Shao 2005; Eslami et al. 2005; Shao and Wang 2006; Ching and Yen 2006; Santos et al. 2008; Poultangari et al. 2008; Ootao 2009; Peng and Li 2010; Malekzadeh and Heydarpour 2012; Heydarpour et al. 2012; Zenkour

✉ Parviz Malekzadeh
malekzadeh@pgu.ac.ir; p_malekz@yahoo.com

¹ Department of Mechanical Engineering, Persian Gulf University, Bushehr 7516913798, Iran

and Sobhy 2013; Dai and Rao 2014). On the other hand, although the accuracy of Fourier heat conduction theory is sufficient for many practical engineering applications, this theory cannot accurately predict the transient temperature field caused by sudden change of the thermal boundary conditions and also laser heating. This is because the Fourier heat conduction law relates the heat flux directly to the temperature gradient using the thermal conductivity. In addition, this conventional heat conduction theory leads to an infinite speed of thermal wave propagation, which is physically unrealistic. To eradicate these deficiencies and improve the accuracy of the traditional heat conduction law and also uncoupled thermoelasticity theory, different generalized thermoelasticity theories have been developed in the past years (Lord and Shulman 1967; Hetnarski and Ignaczak 1999; Chouduri 2007). In this regard, Lord and Shulman (L–S) (Lord and Shulman 1967) have introduced an additional material property, called thermal relaxation time, to consider a finite wave speed for the thermal energy propagation. Based on the generalized coupled thermoelasticity of Lord and Shulman, the temperature field is coupled with the displacement field, and therefore, any attempt to define the temperature distribution within the body should be done with simultaneous consideration of thermoelastic equations (Lord and Shulman 1967).

The static, free vibration and buckling analyses of homogeneous and non-homogeneous plates and shells have been studied extensively in previous works using different numerical techniques (Gürses et al. 2009; Civalek et al. 2010; Baltacıoglu et al. 2010; Xiang et al. 2002; Civalek 2006; Fantuzzi et al. 2017; Tornabene 2009; Tornabene and Viola 2013; Tornabene et al. 2016; Banic et al. 2017; Tornabene et al. 2017). Also, many investigators have conducted the thermoelastic analysis of FG spherical shells based on the classical uncoupled theory of thermoelasticity (Obata and Noda 1994; Eslami et al. 2005; Poultangari et al. 2008; Alavi et al. 2008; Dai et al. 2011; Bayat et al. 2012). But, in comparison with the research works in these topics, to the best of the authors' knowledge, there are only few available studies in the open literature which are concerned with the thermoelastic analysis of single-layer homogeneous and FG spherical shells based on the generalized theories of thermoelasticity (Bagri and Eslami 2007; Ghosh and Kanoria 2008, 2009; Kiani and Eslami 2016; Sharma and Mishra 2017).

Bagri and Eslami (2007) examined the dynamic response of a FG sphere under thermal shock loads. The Galerkin finite element method together with the Laplace transformation was employed to solve the coupled form of the governing equations. A numerical inversion of the Laplace transform was used to obtain the results in the time domain. Ghosh and Kanoria (2008) determined the displacement, stress and temperature distributions in a FG spherically isotropic infinite elastic medium having a spherical cavity under thermal

shock. Also, in another study, they carried out the displacement and stress distributions in a FG spherically isotropic hollow sphere subjected to a time-dependent thermal shock on its inner surface and a prescribed constant temperature on its outer surface (Ghosh and Kanoria 2009). In both mentioned works, the basic equations were written in the form of a vector–matrix differential equation in the Laplace transform domain which was then solved by an eigenvalue approach. The above-mentioned studies are performed based on the Green–Lindsay theory of thermoelasticity which has two relaxation time parameters. Recently, Kiani and Eslami (2016) investigated the thermoelastic response of a thick sphere based on the Lord–Shulman theory of generalized thermoelasticity under thermal shock. They considered the thermally nonlinear term in energy equation. The resulting one-dimensional radial equation of motion and energy equation were discretized by means of the generalized differential quadrature method and Newmark time marching scheme in the radial direction and time domain, respectively. Also, Sharma and Mishra (2017) presented analytical solution for the free vibrations of FG hollow sphere in the context of linear theory of generalized thermoelasticity with one relaxation time (i.e., Lord–Shulman theory).

In the all of the important works reviewed above, the temperature dependence of material properties is neglected, and in addition, the radiation heat transfer from the boundaries of the shell is not considered. On the other hand, to the best of the authors' knowledge, there is no study on the thermoelastic analysis of laminated spherical shells with FG layers in the open literature. Due to the practical importance of this problem, this issue is considered in the present study. In this regard, the coupled equations of the L–S thermoelasticity theory are employed to evaluate the impacts of thermal and stress wave propagation velocity and, consequently, the better simulation of the variation of temperature, displacement and stress components in the FG spherical shells. On the inner and outer surfaces of the shells, both the radiation and convection heat transfer are considered. The material properties are assumed to be temperature dependent and graded in the radial direction. As an efficient and accurate numerical tool, the layerwise-differential quadrature method (LW-DQM) (Heydarpour et al. 2012; Civalek 2004; Malekzadeh et al. 2008, 2012; Malekzadeh and Heydarpour 2013; Talebitooti 2013; Malekzadeh et al. 2014; Heydarpour et al. 2014; Tornabene et al. 2015; Tornabene et al. 2016; Tornabene 2016; Heydarpour and Aghdam 2016; Heydarpour and Aghdam 2016) in conjunction with the Newmark time integration scheme (Reddy 2006) is employed to discretize the governing equations in the spatial and temporal domains, respectively. The resulting nonlinear system of equations is solved using the Newton–Raphson method. After validating the approach, some parametric studies are carried out to investigate the influence of material properties, temperature dependency of material

properties, relaxation time, radiation heat transfer and different geometrical parameters on the nonlinear transient response of the FG laminated spherical shells under thermal loading.

2 Governing Equation

A multilayered FG spherical shell with the inner radius R_i , outer radius R_o and layer thickness h is considered (Fig. 1). Due to the axisymmetric geometry, material properties and loading conditions of the shells under consideration, their field variables become axisymmetric, and consequently, the system of differential equations is reduced to the one-dimensional one.

In order to accurately model the variation of the field variables across the thickness of laminated shells, in the radial direction they are divided into N_m mathematical layers which can be equal to or greater than the number of actual physical layers N_L . It is assumed that the material properties of each physical layer vary continuously and smoothly through-the-thickness direction r such that the inner (outer) surface of each layer is ceramic rich (metal rich) and the outer surface is metal rich (ceramic rich). In this study, the effective material properties are obtained using the power-law distribution. Hence, a typical effective material property ‘ P ’ of the e th layer can be represented as (Heydarpour et al. 2012):

$$P^{(e)}(r, T^{(e)}) = P_i^{(e)}(T^{(e)}) + [P_o^{(e)}(T^{(e)}) - P_i^{(e)}(T^{(e)})] \left(\frac{r - R_i^{(e)}}{R_o^{(e)} - R_i^{(e)}} \right)^p \tag{1}$$

where p denotes the power-law exponent, which is a positive real number, and $P^{(e)}$ and $T^{(e)}$ are the material property and the temperature (in Kelvin) at an arbitrary material

point of the e th layer, respectively. Also, the subscripts i and o , respectively, indicate the material of the inner and outer surfaces of the shell layers. Hereafter, the subscripts m and c are used to signify the metal and ceramic phases of the layers, respectively. For example, if $i = m$ and $o = c$, then the inner surface of the shell layer is metal rich, whereas the outer surface is pure ceramic.

Variation of an arbitrary material property ‘ $Q^{(e)}$ ’ of the e th layer in terms of temperature can be expressed as (Santos et al. 2008):

$$Q^{(e)}(T) = Q_0^{(e)} \left(Q_{-1}^{(e)} T^{-1} + 1 + Q_1^{(e)} T + Q_2^{(e)} T^2 + Q_3^{(e)} T^3 \right) \tag{2}$$

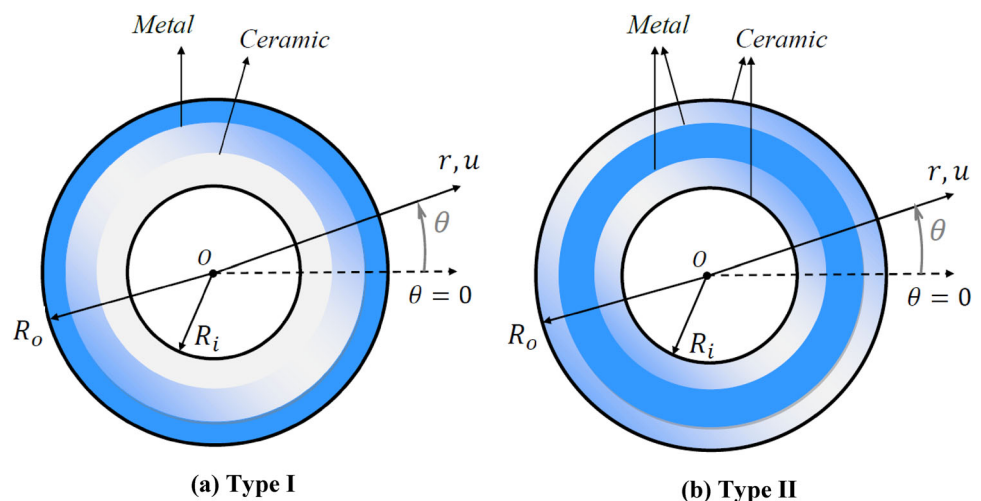
The coefficients $Q_i^{(e)}$ ($i = -1, 0, 1, 2, 3$) are unique for each material.

Based on the linear elasticity theory, the constitutive relations at an arbitrary material point of the e th shell layer can be written as:

$$\begin{Bmatrix} \sigma_{rr}^{(e)} \\ \sigma_{\theta\theta}^{(e)} \\ \sigma_{\phi\phi}^{(e)} \end{Bmatrix} = \begin{bmatrix} c_{11}^{(e)} & c_{12}^{(e)} & c_{12}^{(e)} \\ c_{12}^{(e)} & c_{11}^{(e)} & c_{12}^{(e)} \\ c_{12}^{(e)} & c_{12}^{(e)} & c_{11}^{(e)} \end{bmatrix} \begin{Bmatrix} \frac{\partial u^{(e)}}{\partial r} - \int_{T_0}^{T^{(e)}} \alpha^{(e)} dT \\ \frac{u^{(e)}}{r} - \int_{T_0}^{T^{(e)}} \alpha^{(e)} dT \\ \frac{u^{(e)}}{r} - \int_{T_0}^{T^{(e)}} \alpha^{(e)} dT \end{Bmatrix} \tag{3}$$

where $\sigma_{ii}^{(e)}$ ($i = r, \theta, \phi$) are the normal stress tensor components in which r, θ and ϕ are the conventional coordinate variables of the spherical coordinate system; $u^{(e)}$ is the radial displacement component at an arbitrary material point of the e th layer; $\alpha^{(e)} [= \alpha^{(e)}(r, T^{(e)})]$ is the thermal expansion coefficient; and T_0 is the reference temperature,

Fig. 1 a, b Two different types of laminated FG hollow spherical shells



i.e., the temperature at which the shell is stress free; also, $c_{ij}^{(e)} [= c_{ij}^{(e)}(r, T^{(e)}) ; i, j = 1, 2]$ are the material elastic coefficients at an arbitrary material point of the shell (Ghosh and Kanoria 2008).

It is assumed that the spherical shell has an initial temperature distribution T_0 and then suddenly exchanges heat through its inner and outer boundaries with the inside and outside mediums. Due to the axisymmetric geometry, thermal loading conditions and also the material properties, the governing equations become independent of θ and ϕ coordinate variable coordinates. Hence, in each layer, the equation of balance of energy and equation of motion based on the L–S theory can be expressed as (Lord and Shulman 1967), respectively Energy equation:

$$\rho^{(e)} c^{(e)} \left(\frac{\partial T^{(e)}}{\partial t} + \tau_0^{(e)} \frac{\partial^2 T^{(e)}}{\partial t^2} \right) + \alpha^{(e)} (3\lambda^{(e)} + 2\mu^{(e)}) \left(\tau_0^{(e)} \frac{\partial^2}{\partial t^2} + \frac{\partial}{\partial t} \right) \left(\frac{\partial u^{(e)}}{\partial r} + \frac{2u^{(e)}}{r} \right) = \frac{1}{r^2} \frac{\partial}{\partial r} \left(r^2 k^{(e)} \frac{\partial T^{(e)}}{\partial r} \right) \tag{4}$$

Equation of motion:

$$\frac{\partial \sigma_{rr}^{(e)}}{\partial r} + \frac{2(\sigma_{rr}^{(e)} - \sigma_{\theta\theta}^{(e)})}{r} = \rho^{(e)} \frac{\partial^2 u^{(e)}}{\partial t^2} \tag{5}$$

where $e = 1, 2, \dots, N_m$; also, $k^{(e)} [= k^{(e)}(r, T)]$ is the thermal conductivity, $\rho^{(e)} [= \rho^{(e)}(r, T)]$ is the mass density, $c^{(e)} [= c^{(e)}(r, T)]$ is the specific heat capacity, $\tau_0^{(e)}$ is the relaxation time of the L–S model, $\lambda^{(e)}$ and $\mu^{(e)}$ is the Lamé constants of material surface (r) of the e th layer and t is the time.

Among the different thermal boundary conditions that can be considered at the surfaces of the spherical shell, the convection–radiation thermal conditions are assumed on the inner and outer surfaces of the shell

$$\begin{aligned} \text{At } r = R_i^{(1)} : & -k^{(1)} \frac{\partial T^{(1)}}{\partial \bar{r}} \\ & = h_{ci} (T_{\infty i} - T^{(1)}) + \varepsilon \sigma \left[T_{\infty i}^4 - (T^{(1)})^4 \right], \\ \text{At } r = R_o^{(N_m)} : & -k^{(N_m)} \frac{\partial T^{(N_m)}}{\partial \bar{r}} \\ & = h_{co} (T^{(N_m)} - T_{\infty o}) + \varepsilon \sigma \left[(T^{(N_m)})^4 - T_{\infty o}^4 \right] \end{aligned} \tag{6a, b}$$

where $T_{\infty i}$ and $T_{\infty o}$ are the temperature of the inner and outer mediums, respectively, which are assumed to be constant; h_{ci} and h_{co} denote the convective heat transfer coefficients of the inside and outside media of the shell, respectively; σ refers to the Boltzmann constant; and ε is the emissivity coefficient. Also, the following thermal initial conditions are considered

$$T^{(e)}(r, 0) = T_0, \left. \frac{\partial T^{(e)}(r, t)}{\partial t} \right|_{t=0} = 0 \tag{7a, b}$$

The mechanical boundary conditions at the inner and outer surfaces of the shells $[r = R_i^{(1)}, R_o^{(N_m)}]$, which are assumed to be stress free, and also their initial conditions are as follows:

Mechanical boundary conditions (traction free surface boundaries):

$$\begin{aligned} \text{At } r = R_i^{(1)} : & \left[C_{11}^{(1)} \frac{\partial u^{(1)}}{\partial r} + 2C_{12}^{(1)} \frac{u^{(1)}}{r} - (C_{11}^{(1)} + 2C_{12}^{(1)}) \left(\int_{T_0}^{T^{(1)}} \alpha^{(1)} dT \right) \right] = 0, \\ \text{At } r = R_o^{(N_m)} : & \left[C_{11}^{(N_m)} \frac{\partial u^{(N_m)}}{\partial r} + 2C_{12}^{(N_m)} \frac{u^{(N_m)}}{r} - (C_{11}^{(N_m)} + 2C_{12}^{(N_m)}) \left(\int_{T_0}^{T^{(N_m)}} \alpha^{(N_m)} dT \right) \right] = 0 \end{aligned} \tag{8a, b}$$

Mechanical initial conditions:

$$u^{(e)}(r, 0) = 0, \left. \frac{\partial u^{(e)}(r, t)}{\partial t} \right|_{t=0} = 0 \tag{9a, b}$$

In addition to the above boundary and initial conditions, the geometrical and natural compatibility conditions at the interface of the two adjacent shell layers should be implemented to allow one to uniquely determine the temperature distribution and the displacement component in the layered shells. These continuity conditions at the interface of two adjacent layers of the multilayered spherical shell take the following form: Thermal compatibility conditions:

$$\begin{aligned} T^{(e)}(R_o^{(e)}) & = T^{(e+1)}(R_i^{(e+1)}), \\ \left[k^{(e)}(r) \frac{\partial T^{(e)}}{\partial r} \right]_{r=R_o^{(e)}} & = \left[k^{(e+1)}(r) \frac{\partial T^{(e+1)}}{\partial r} \right]_{r=R_i^{(e+1)}} \end{aligned} \tag{10a, b}$$

Mechanical compatibility conditions:

$$\begin{aligned} u^{(e)}(R_o^{(e)}) & = u^{(e+1)}(R_i^{(e+1)}), \\ \left[C_{11}^{(e)} \frac{\partial u^{(e)}}{\partial r} + 2C_{12}^{(e)} \frac{u^{(e)}}{r} - (C_{11}^{(e)} + 2C_{12}^{(e)}) \left(\int_{T_0}^{T^{(e)}} \alpha^{(e)} dT \right) \right]_{r=R_o^{(e)}} & = \\ \left[C_{11}^{(e+1)} \frac{\partial u^{(e+1)}}{\partial r} + 2C_{12}^{(e+1)} \frac{u^{(e+1)}}{r} - (C_{11}^{(e+1)} + 2C_{12}^{(e+1)}) \left(\int_{T_0}^{T^{(e+1)}} \alpha^{(e+1)} dT \right) \right]_{r=R_i^{(e+1)}} & \end{aligned} \tag{11a, b}$$

where $e = 1, 2, \dots, N_m - 1$.

3 Solution Procedure

Due to the fact that the governing differential equations have variable coefficients and also the governing differential equation of energy balance and the related boundary conditions are nonlinear, it is difficult to solve them analytically. Hence, an appropriate numerical method should be employed to find the solution. In this work, the layerwise-differential quadrature method (LW-DQM) as an accurate and efficient numerical tool (Heydarpour et al. 2012; Civalek 2004; Malekzadeh et al. 2008, 2012; Malekzadeh and Heydarpour 2013; Talebitooti 2013; Malekzadeh et al. 2014; Heydarpour et al. 2014; Tornabene et al. 2015; Tornabene et al. 2016; Tornabene 2016; Heydarpour and Aghdam 2016; Heydarpour and Aghdam 2016) in conjunction with Newmark’s time integration scheme (Reddy 2006) is adopted to discretize the governing equations in the spatial and time domains, respectively. According to this method, each mathematical layer of the shell is discretized into a set of $N_r^{(e)}$ grid points along the radial direction. Then, the spatial derivatives in the differential equations are discretized at the domain grid points. More details of the differential quadrature method (DQM) can be found in the interesting review paper of Tornabene et al. (2015). For the sake of brevity, the differential quadrature (DQ) discretized form of the balance of energy Eq. (4) for the e th layer is presented here

$$\begin{aligned} & \rho_i^{(e)} c_i^{(e)} \left(\frac{dT^{(e)}}{dt} + \tau_0^{(e)} \frac{d^2 T^{(e)}}{dt^2} \right)_i + \alpha_i^{(e)} \left(3\lambda_i^{(e)} + 2\mu_i^{(e)} \right) \\ & T_0 \left(\tau_{0i}^{(e)} \frac{d^2}{dt^2} + \frac{d}{dt} \right) \left(\sum_{m=1}^{N_r^{(e)}} A_{im}^{(er)} u_m^{(e)} + \frac{2u_i^{(e)}}{r_i} \right) = \\ & k_i^{(e)} \sum_{m=1}^{N_r^{(e)}} B_{im}^{(er)} T_m^{(e)} + \left(\frac{dk^{(e)}}{dr} + \frac{2k^{(e)}}{r} \right) \sum_{i,m=1}^{N_r^{(e)}} A_{im}^{(er)} T_m^{(e)} \end{aligned} \quad (12)$$

where $i = 2, \dots, \hat{N}_r^{(e)} (= N_r^{(e)} - 1)$ and $A_{im}^{(e)}$ and $B_{im}^{(e)}$ refer to the weighting coefficients of the first- and second-order

DQM weighting coefficients (Malekzadeh et al. 2012). In a similar manner, the other differential equations and the related boundary and compatibility conditions can be discretized. After doing these, one gets a system of nonlinear ordinary differential equations as

$$[M] \left\{ \frac{d^2 D}{dt^2} \right\} + [C] \left\{ \frac{dD}{dt} \right\} + [K] \{D\} = \{f(t)\} \quad (13)$$

where $\{D\}$ is the vector of degrees of freedom (i.e., the temperature and the radial displacement of the grid points); also, $[M]$, $[C]$ and $[K]$ are the mass, thermoelastic damping and stiffness matrices, respectively. In order to solve the system of ordinary differential Eq. (13) in the time domain, the Newmark’s time integration scheme (Reddy 2006) is employed. Afterward, one obtains a system of nonlinear algebraic equations in each time interval. In this work, Newton–Raphson method is employed to solve this system of nonlinear algebraic equations in each time step and the procedure is repeated for all time intervals. At the end of each time interval, the obtained temperature and displacement component are used as the initial conditions for the next time step. Finally, the temperature distribution together with the displacement and stress components is obtained in each time step and at any grid point of the FG spherical shell.

4 Numerical Results

In this section, after validating the present formulation and solution technique for the transient thermoelastic analysis of laminated spherical shells with FG layers subjected to thermal loading, some parametric studies are carried out. Two common types of FG sandwich shells are considered. Type I consists of FG core surrounded by homogeneous inner and outer layers (Fig. 1a), while type II is made of

Table 1 Temperature-dependent coefficients of material properties for zirconia (ZrO₂) and stainless steel (AISI 304) (Santos et al. 2008)

| | Material | Q_{-1} | Q_0 | Q_1 | Q_2 | Q_3 |
|-----------------------------|-----------------|----------|-------------------------|-------------------------|-------------------------|--------------------------|
| E (Pa) | Stainless steel | 0 | 201.04×10^9 | 3.079×10^{-4} | -6.534×10^{-7} | 0 |
| | Zirconia | 0 | 244.27×10^9 | -1.371×10^{-3} | 1.214×10^{-6} | -3.681×10^{-10} |
| ν | Stainless steel | 0 | 0.3262 | -2.002×10^{-4} | 3.797×10^{-7} | 0 |
| | Zirconia | 0 | 0.2882 | 1.133×10^{-4} | 0 | 0 |
| ρ (kg/m ³) | Stainless steel | 0 | 8166 | 0 | 0 | 0 |
| | Zirconia | 0 | 5700 | 0 | 0 | 0 |
| α (1/K) | Stainless steel | 0 | 12.330×10^{-6} | 8.086×10^{-4} | 0 | 0 |
| | Zirconia | 0 | 12.766×10^{-6} | -1.491×10^{-3} | 1.006×10^{-5} | -6.778×10^{-11} |
| k (W/m K) | Stainless steel | 0 | 15.379 | -1.264×10^{-3} | 2.092×10^{-6} | -7.223×10^{-10} |
| | Zirconia | 0 | 1.700 | 1.276×10^{-4} | 6.648×10^{-8} | 0 |
| c (J/kgK) | Stainless steel | 0 | 496.56 | -1.151×10^{-3} | 1.636×10^{-6} | -5.863×10^{-10} |
| | Zirconia | 0 | 487.34 | 3.049×10^{-4} | -6.037×10^{-8} | 0 |

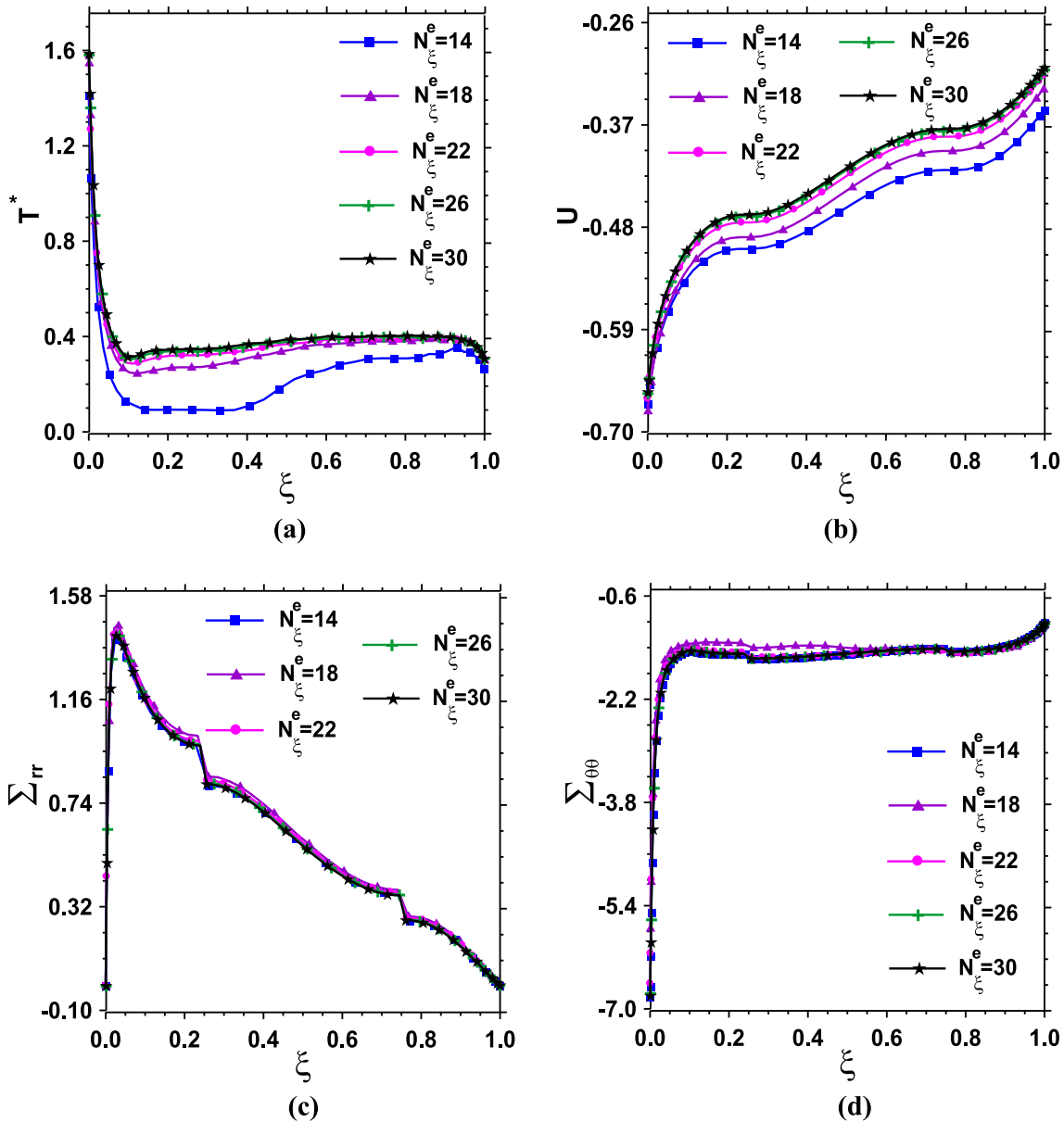


Fig. 2 a–d Convergence of the results against the number of DQ grid points for the spherical shells of type II ($F_o = 0.2, p = 1, \tau = 0.1, \lambda = 0.1, N_i = 400$)

FG inner/outer layers with homogeneous core (Fig. 1b). The individual layers are assumed to have equal thickness and are composed of zirconia (ceramic) and stainless steel (metal) (Santos et al. 2008). The material properties of zirconia (ZrO_2) and stainless steel (AISI 304) are given in Table 1. Three mathematical layers are used to model these shells in the thickness direction. Also, unless otherwise specified, in all case studies, the material properties are assumed to be temperature dependent and the following values are used for the other parameters: $R_i = 1.4$ (m), $R_o = 2$ (m), $T_0 = T_{\infty o} = 300$ (K), $T_{\infty i} = 1000$ (K) and $h_{ci} = h_{co} = 10$ (W/m²K). Also, the non-dimensional parameters are defined as:

$$\begin{aligned}
 F_o &= \frac{tk_{0m}}{\rho c_{0m} R_o^2}, & \lambda &= \frac{R_o \varepsilon \sigma T_{\infty}^3}{k_{0m}}, & \tau &= \frac{\tau_0 \tilde{\alpha}}{R_o^2}, \\
 T^* &= \frac{T - T_{\infty}}{T_{\infty}}, & U &= \frac{h}{(1 + \nu_{0m}) \alpha_{0m} T_{\infty} R_o^2} u \\
 \zeta &= \frac{r - R_i}{R_o - R_i}, & \Sigma_{ii} &= \frac{(1 + \nu_{0m}) h}{R_o E_{0m} \alpha_{0m} T_{\infty}} \sigma_{ii} \text{ with } i = r, \theta.
 \end{aligned}
 \tag{14a-h}$$

where $\tilde{\alpha}(= k/\rho c)$ is the thermal diffusivity of the FG shell.

As a first example, the convergence behavior of the non-dimensional results of sandwich shell of type II under

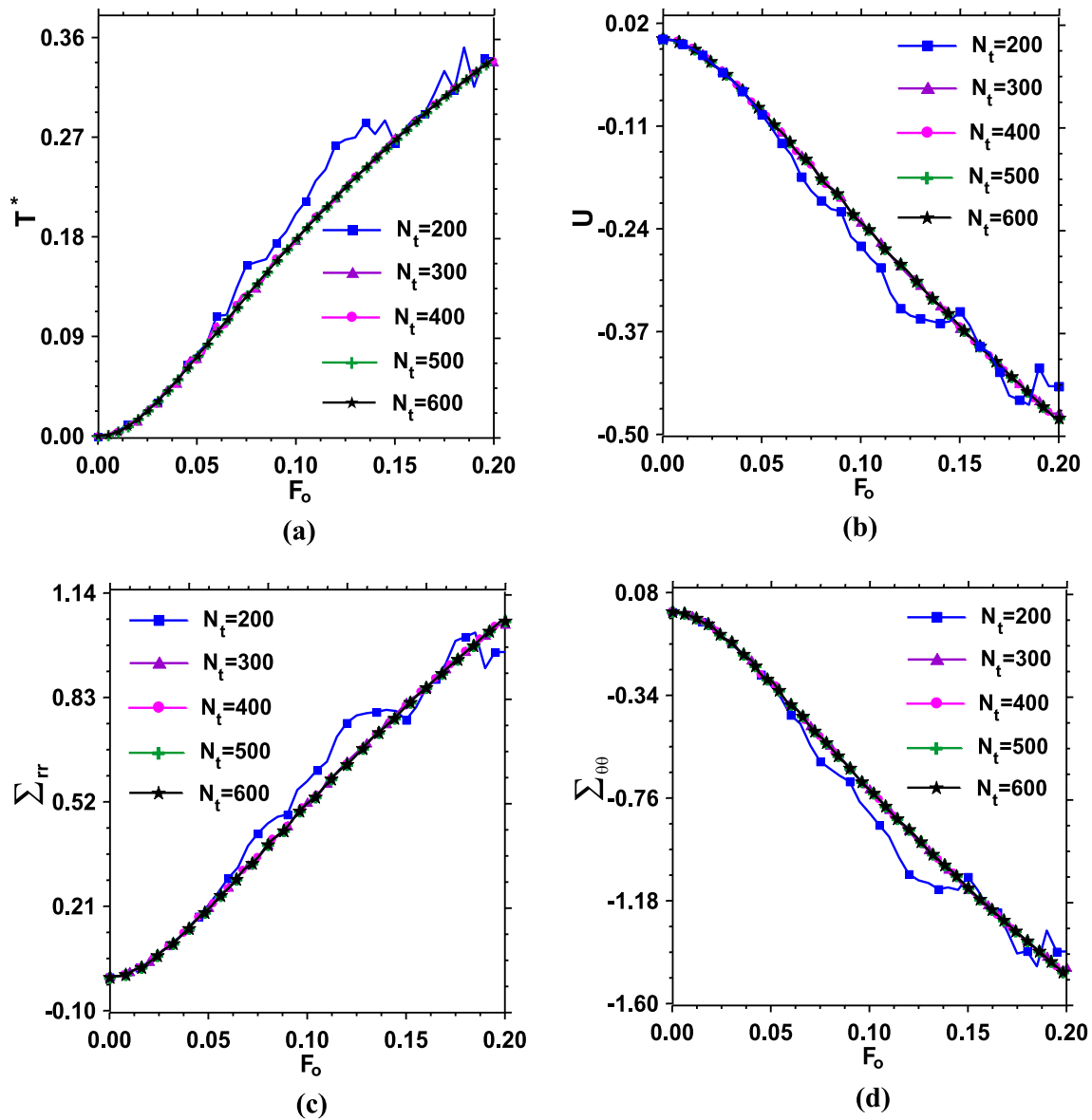


Fig. 3 a–d Convergence of the results against the number of time steps for the spherical shells of type II ($p = 1$, $\tau = 0.1$, $\lambda = 0.1$, $\xi = 0.25$, $N_\xi^{(e)} = 30$)

thermal loading against the DQ number of grid points along the thickness direction ($N_\xi^{(e)} = N_r^{(e)}$) and the number of time steps are carried out and are shown in Figs. 2 and 3, respectively. The fast rate of convergence and numerical stability of the results are clear, and one can observe that thirty DQ grid points per layer yield converged results.

In order to clarify the accuracy of the presented formulation and method of solution, the non-Fourier heat conduction of a FG spherical shell subjected to a sudden temperature change on its outer surface, which has been analytically analyzed by Akbarzadeh and Chen (2014), is considered. The results for the temperature distribution within the shell based on the non-Fourier and Fourier heat conduction theories are compared with Akbarzadeh and

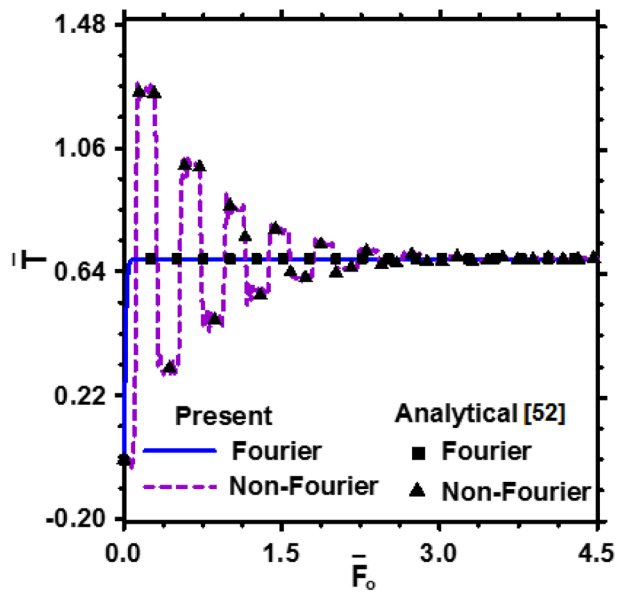


Fig. 4 Comparison of the non-dimensional temperature of an FG hollow sphere subjected to a sudden temperature change on the outer surface based on the non-Fourier and Fourier heat conduction theories. ($\zeta = 0.8$, $\bar{\tau} = 0.35$)

Chen (2014) in Fig. 4. The material properties vary radially according to the following power-law formulation:

$$\psi = \psi_0 r^n \tag{15}$$

where ψ_0 denotes the material constant at the outer surface and n is the non-homogeneity index. The geometrical and heat transfer parameters are: $R_i = 0.6$ (m), $R_o = 1$ (m), $T_{wi} = T_\infty = 300$ K and $T_{wo} = 500$ K. Also, similar non-dimensional parameters, thermal and initial boundary conditions at the inner and outer surfaces of the sphere as those in Ref. (Akbarzadeh and Chen 2014) are chosen, which are:

$$\begin{aligned} \bar{F}_0 &= \frac{tk_0}{\rho_0 c_0 R_o^2}, \quad \bar{\tau} = \frac{\tau_0 \bar{\alpha}}{R_o^2}, \quad \bar{T} = \frac{T - T_\infty}{T_{wo} - T_\infty}, \\ T(R_i, t) &= T_{wi}, \quad T(R_o, t) = T_{wo}, \quad T(r, 0) = T_\infty \\ \frac{\partial T}{\partial t} &= 0 \text{ at } t = 0 \end{aligned} \tag{16a-g}$$

where $\bar{\alpha} (= k_0/\rho_0 c_0)$ is the thermal diffusivity. From Fig. 4, excellent agreement of the present work results with the analytical solution (Akbarzadeh and Chen 2014) is observed. Hence, it can be concluded that the method can

accurately predict the thermal wave propagation in the spherical shells.

As another study to examine the accuracy of the method, the non-dimensional temperature distribution, radial displacement and stress components of the FG hollow spherical shells subjected to internal pressure in thermal environment are compared with those of the exact solution obtained by Eslami et al. (2005) in Fig. 5. To find such a solution, all the material properties of the sphere, except Poisson’s ratio, vary according to Eq. (15). The material properties, non-dimensional parameters and boundary conditions of the FG hollow sphere in this example are, respectively (Eslami et al. 2005):

$$\begin{aligned} \nu &= 0.3, \quad E_0 = 200 \text{ (GPa)}, \quad \alpha_0 = 1.2 \times 10^{-6} \left(\frac{1}{^\circ\text{C}} \right); \\ \hat{T} &= \frac{T}{T(R_i)}, \quad \hat{u} = \frac{u}{R_i}, \quad \hat{\sigma}_{jj} = \frac{\sigma_{jj}}{\sigma_{rr}(R_i)} \text{ with } j = r, \theta; \\ T(R_i, t) &= 10 \text{ (}^\circ\text{C)}, \quad T(R_o, t) = 0 \text{ (}^\circ\text{C)}, \\ \sigma_{rr}(R_i, t) &= -50 \text{ (MPa)}, \quad \sigma_{rr}(R_o, t) = 0 \end{aligned} \tag{17a-h}$$

It can be seen that for different values of the material graded index (n), the results of the present approach are in close agreement with the exact solution of Eslami et al. (2005).

After showing the convergence and accuracy of the present approach, parametric studies for the two types of laminated FG spherical shells subjected to thermal loading are carried out. In all solved examples, 400 time steps and thirty grid points per layer in the radial direction are used to generate the numerical results.

The effects of material properties on the thermal wave propagation in the single-layer spherical shells are studied by showing the results for spherical shells made of metal, ceramic and FG materials in Figs. 6, 7, 8, respectively. From these figures, one can see that the propagation of thermal wave for spherical shell made of metal is more obvious than those of shells with ceramic and FG materials.

In Figs. 9, 10, 11, the effects of material properties on the thermo-mechanical behavior of the single- and multi-layer spherical shells are studied. For this purpose, in Fig. 9 comparison between the through-the-thickness variations of the non-dimensional thermo-mechanical field variables (i.e., the non-dimensional temperature distribution, radial displacement and stress components) of a single-layer FG spherical shell (with inner face ceramic and outer face

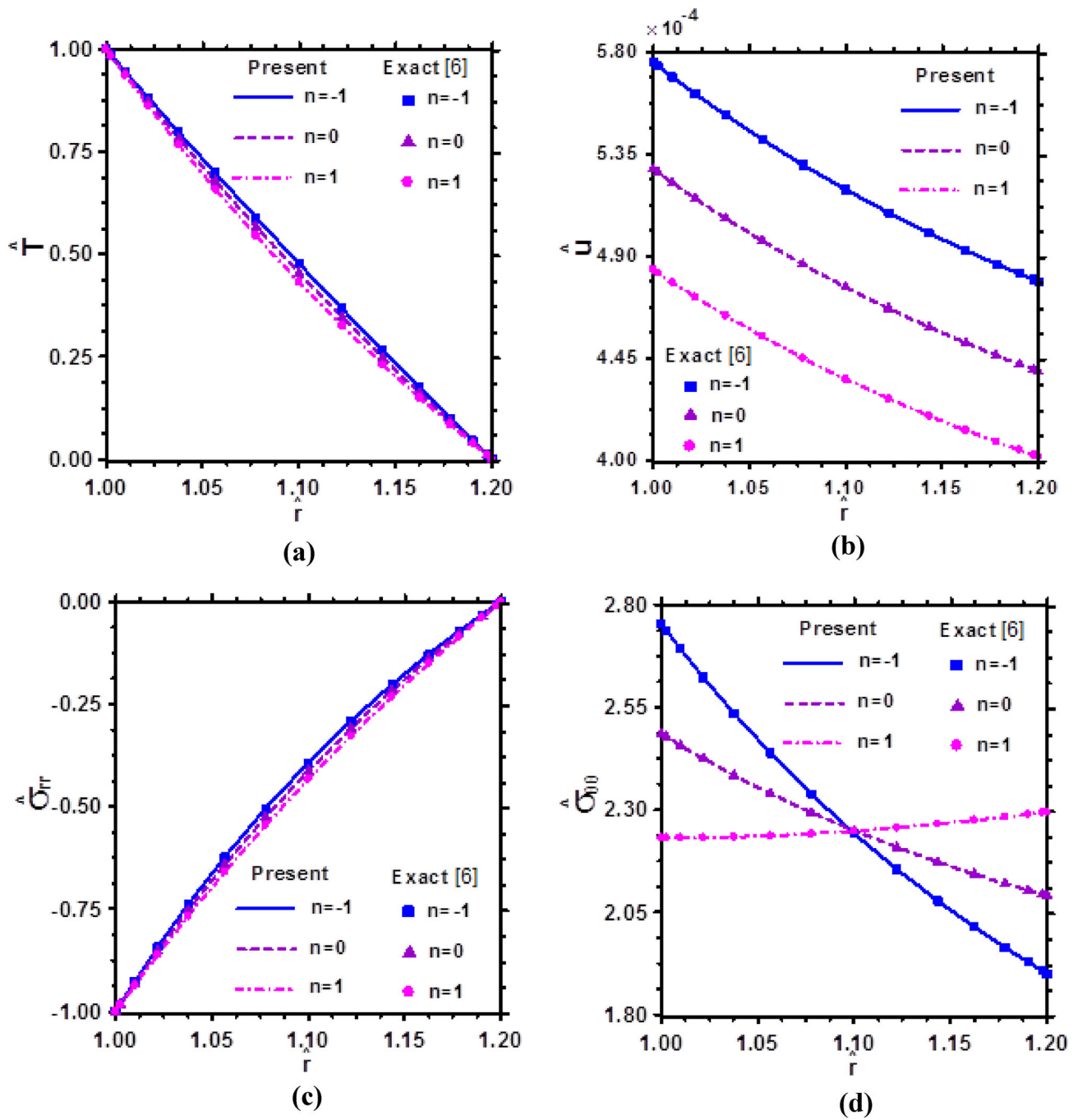


Fig. 5 a–d Comparison of results across the thickness of a FG hollow sphere subjected to internal pressure in thermal environment [$R_i = 1$ (m), $R_o = 1.2$ (m)]

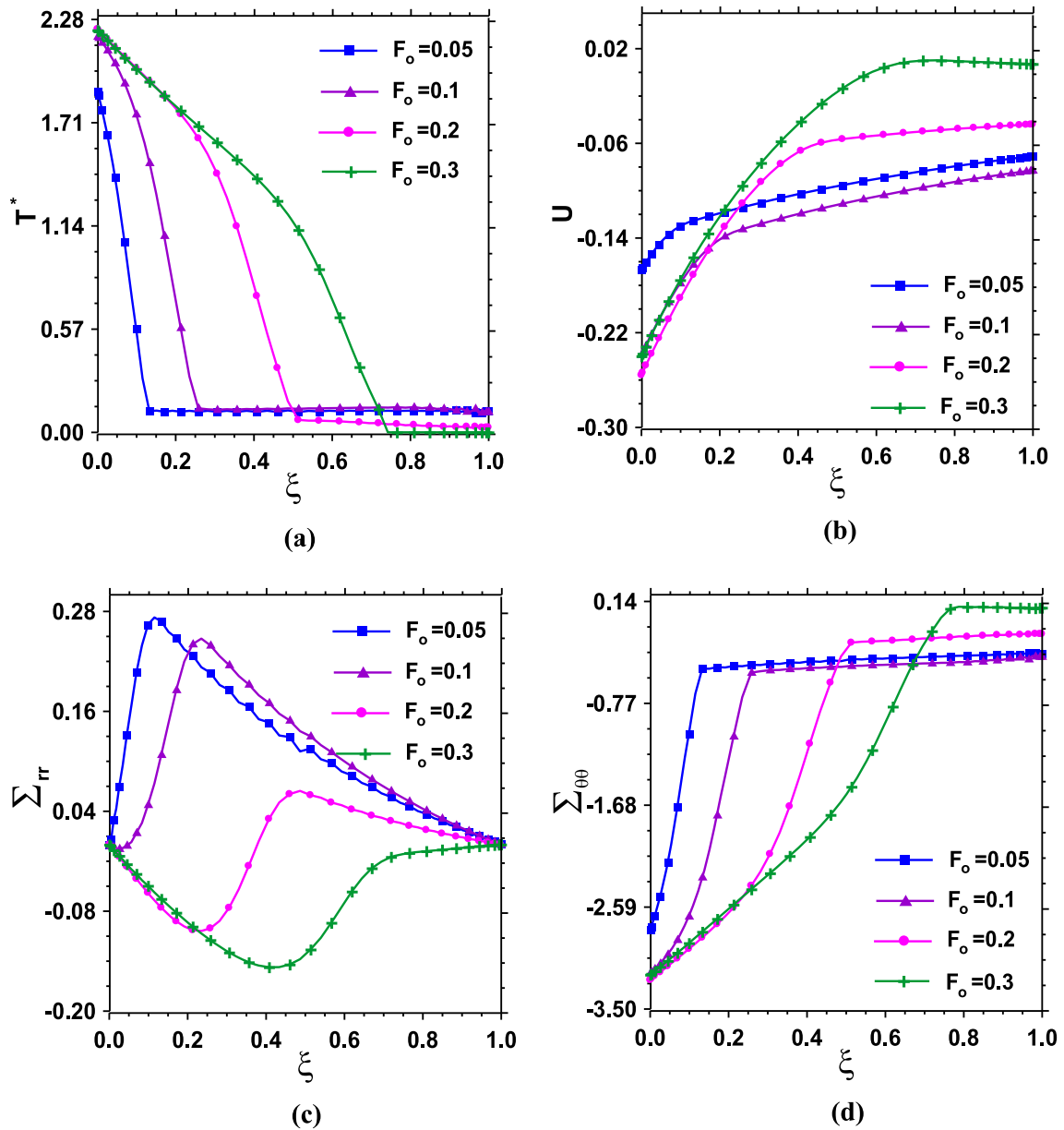


Fig. 6 a–d The wave propagation through the radial direction for spherical shells made of metal ($p = 1$, $\tau = 0.2$, $\lambda = 0.5$)

metal), types I and II of layered spherical shells are done. It seems that the layered shell of type II has better thermo-mechanical performance than the other ones. This is because among the three types of shells, this type has the lowest radial displacement and minimum stress compo-

nents. Also, the influence of the material graded index (p) on the time histories of the thermo-mechanical field variables of the types I and II of spherical shells is shown in Figs. 10 and 11, respectively. It can be seen that in all cases there are considerable differences between the results of

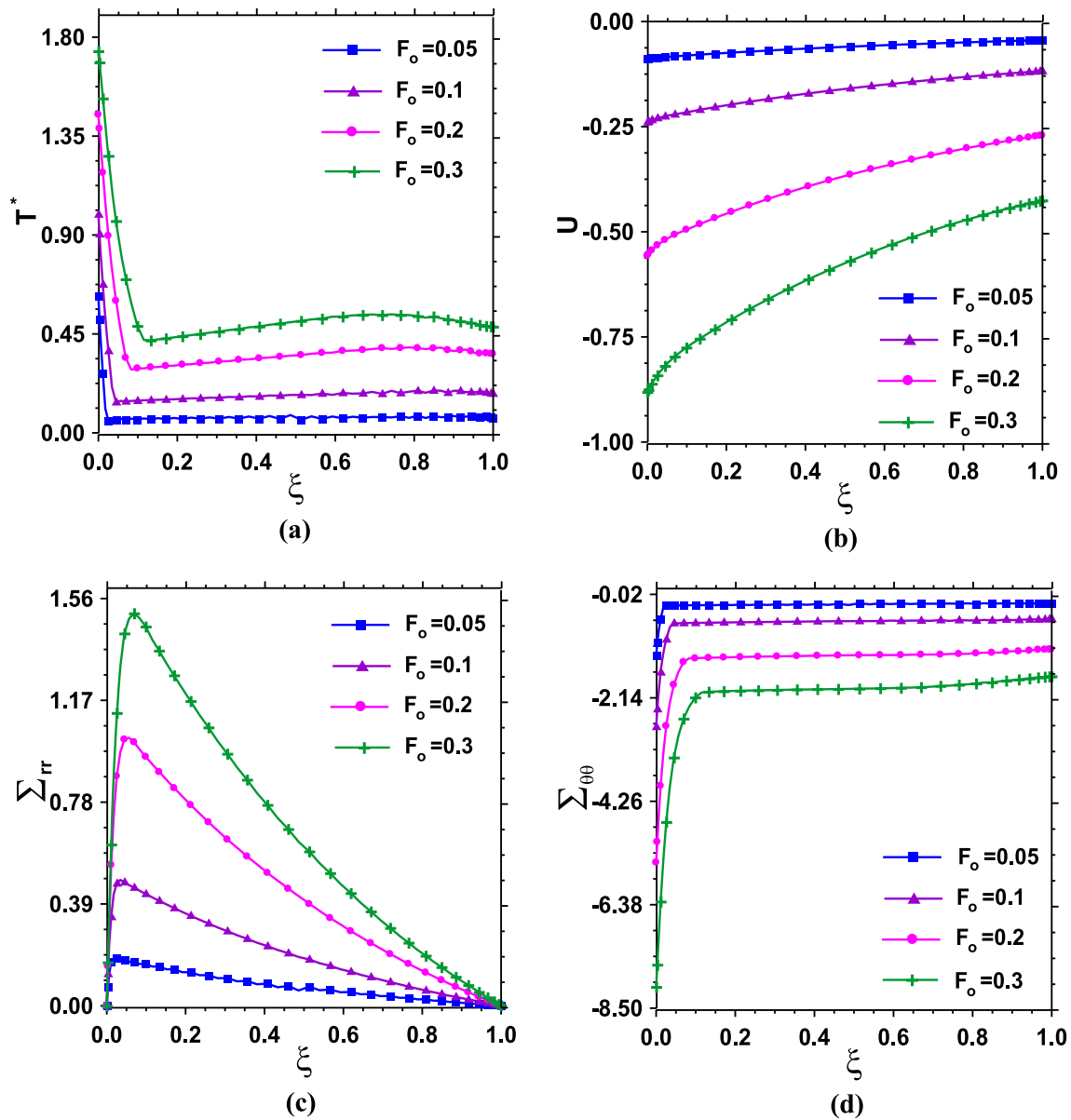


Fig. 7 a–d The wave propagation through the radial direction for spherical shells made of ceramic ($p = 1, \tau = 0.2, \lambda = 0.1$)

the homogeneous ($p = 0$) and non-homogenous ($p = 1$) spherical shells. These differences are more obvious for the type II of FG shells which have metal core than type I with FG core.

The effects of relaxation time on the time histories and the distribution of the non-dimensional thermo-mechanical

field variables through the radial direction of the spherical shells of type II are exhibited in Figs. 12 and 13, respectively. It can be seen that by increasing the relaxation time, the non-dimensional temperature, radial displacement and stress components decrease. However, the relaxation time does not change the variation patterns of these parameters

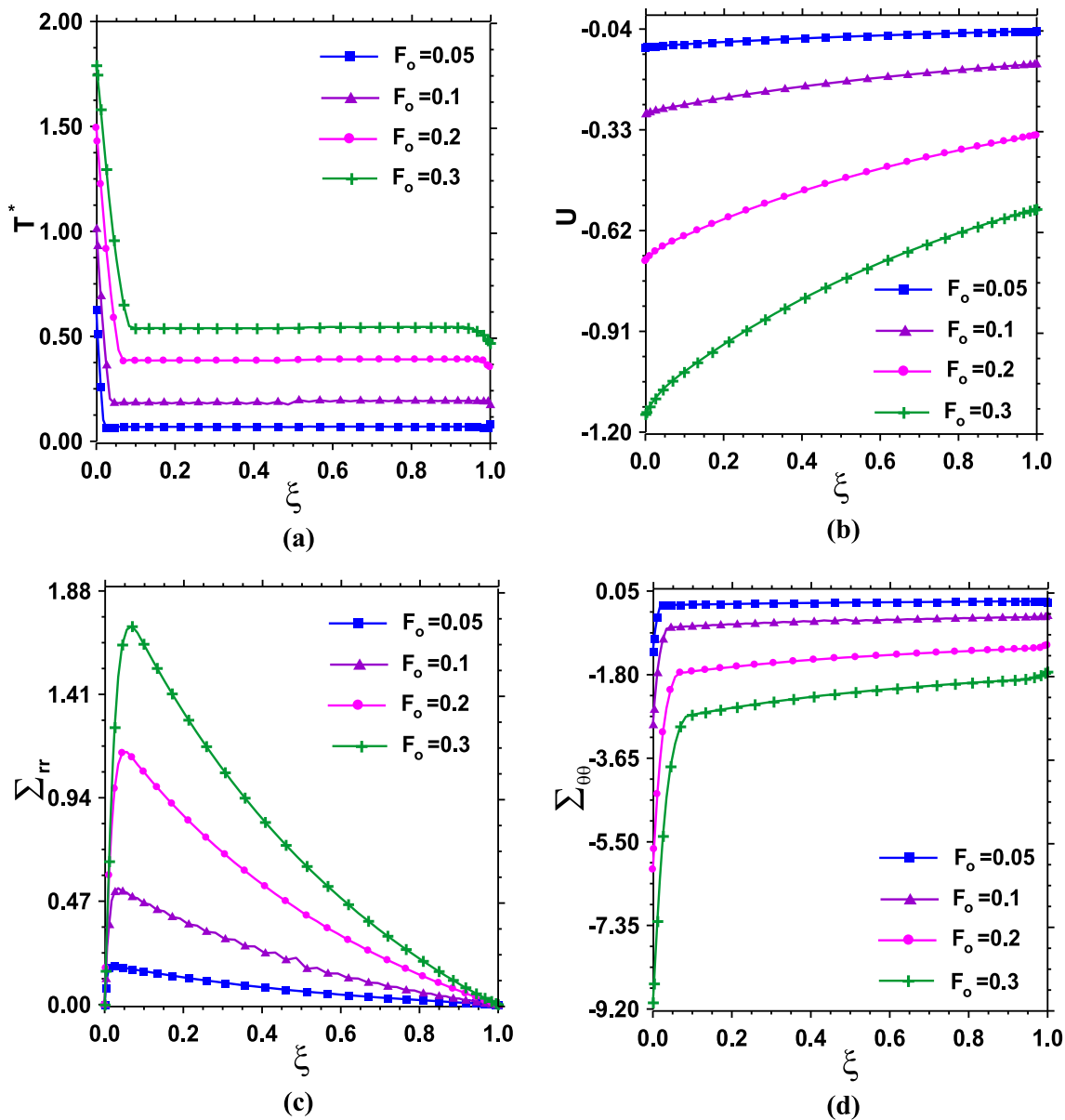


Fig. 8 a–d The wave propagation through the radial direction for a single-layer FG spherical shell ($p = 1$, $\tau = 0.2$, $\lambda = 0.1$)

considerably. Figure 14 depicts the through-the-thickness variations of the non-dimensional thermo-mechanical field variables for the spherical shells of type II at different time levels. It is evident that by increasing the time level, the field variables increase.

The influences of temperature dependence of material properties on the time histories of the results for the spherical shells of type II are studied in Fig. 15. As it can be observed, the temperature dependence of material properties significantly changes the thermo-mechanical

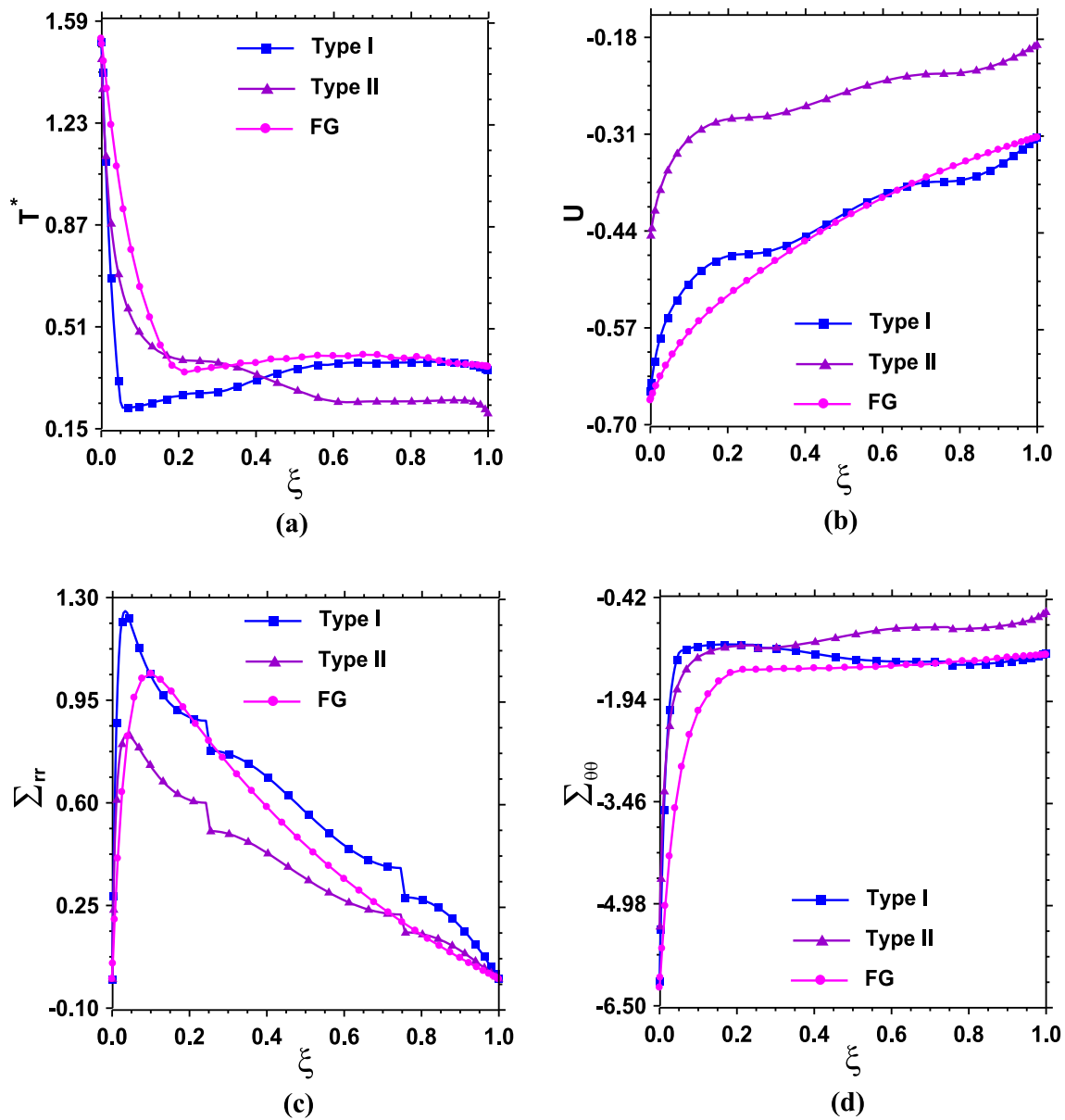


Fig. 9 a–d Comparison of the results for three different types of hollow spherical shells ($F_o = 0.3$, $p = 1$, $\tau = 0.1$, $\lambda = 0.05$)

behavior of the system and cannot be ignored. It is obvious that all of the non-dimensional field variables increase when the temperature dependence of material properties is considered.

In Fig. 16, comparisons between the across-the-thickness variations of the non-dimensional field variables for the spherical shells of type II based on the uncoupled and coupled thermoelasticity theories are performed. One can

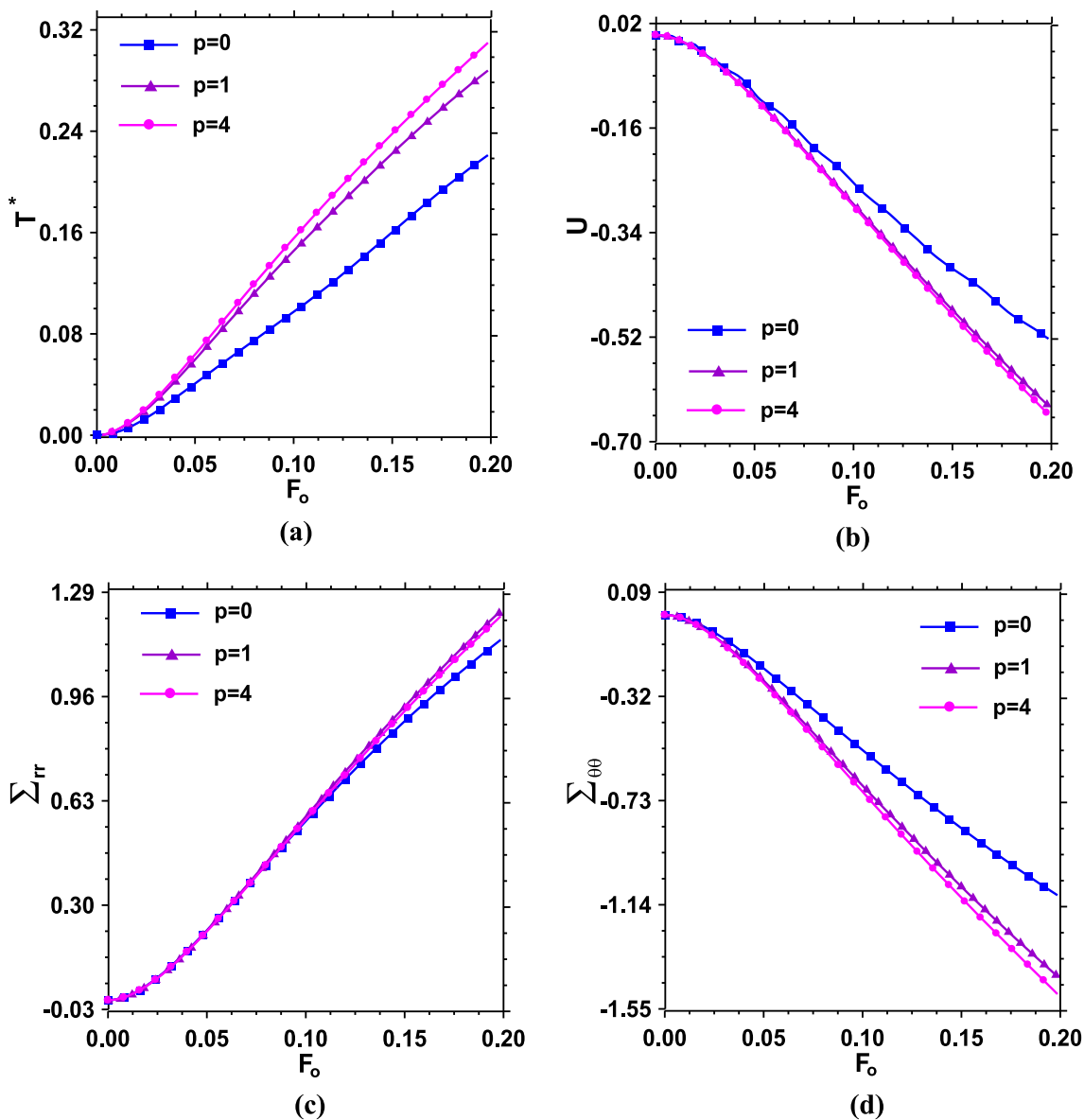


Fig. 10 a–d Time histories of the results against the material graded index (p) for type I spherical shells ($\tau = 0.1$, $\xi = 0.25$, $\lambda = 0.1$)

find that the uncoupled thermoelasticity overpredicts the non-dimensional temperature and radial displacement distribution in the shell. In addition, there are large discrepancies between the stress components obtained according to these theories.

Figure 17 depicts the effects of the thickness-to-outer radius ratio, as an important geometrical parameter, on the time histories of the non-dimensional field variables for the spherical shells of type II. It is interesting to note that all of the field variables, except the radial stress component,

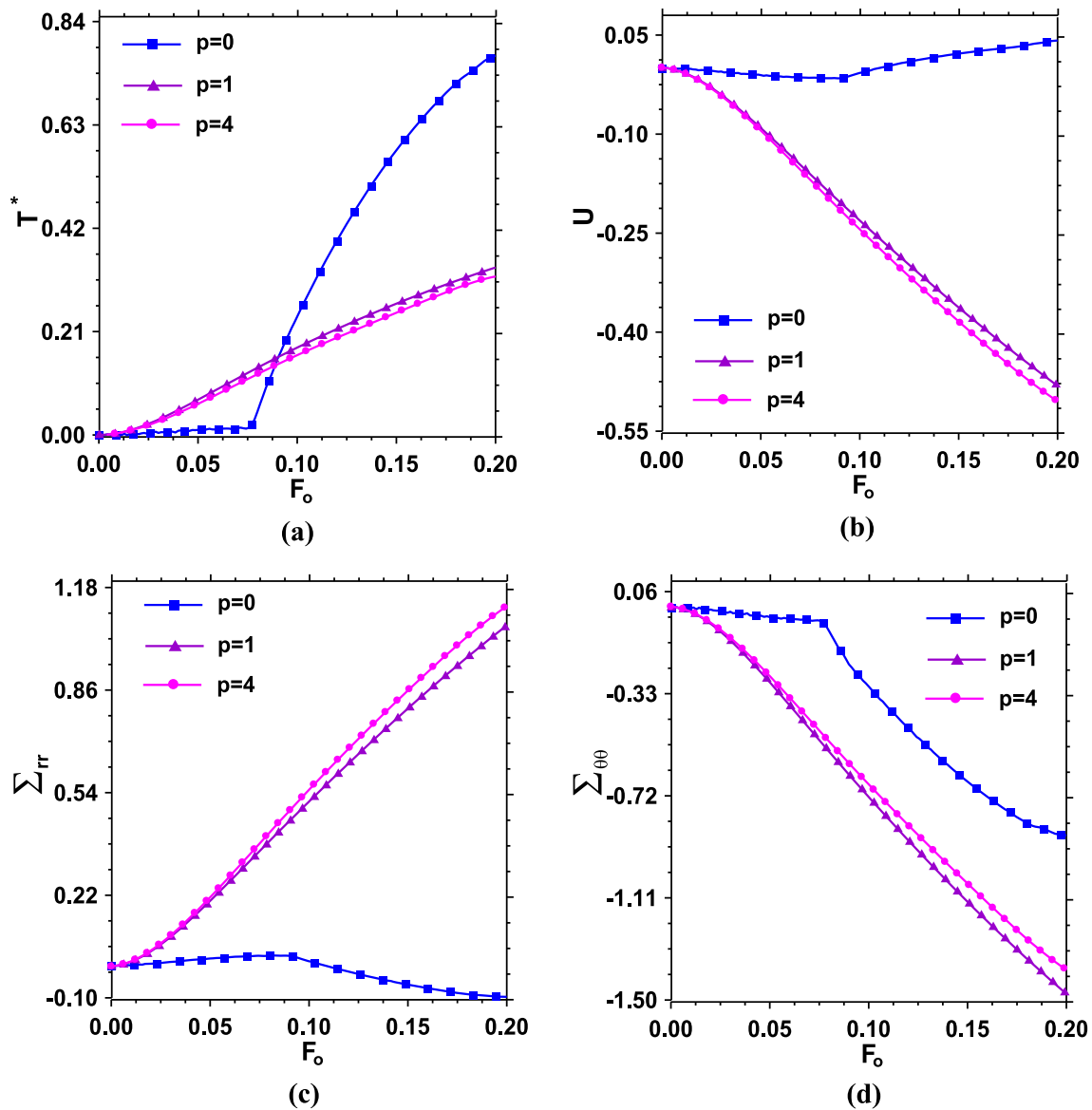


Fig. 11 a–d Time histories of the results against the material graded index (p) for type II spherical shells ($\tau = 0.1$, $\xi = 0.25$, $\lambda = 0.1$)

decrease by increasing the thickness-to-outer radius ratio. However, the radial stress component increases by increasing this geometrical parameter.

5 Conclusion

The transient thermoelastic analysis of multilayered spherical shells with FG layers under the radiative-convective thermal boundary conditions was presented based on the generalized coupled thermoelasticity of Lord–Shulman. The material properties were assumed to be temperature dependent and graded in the radial direction.

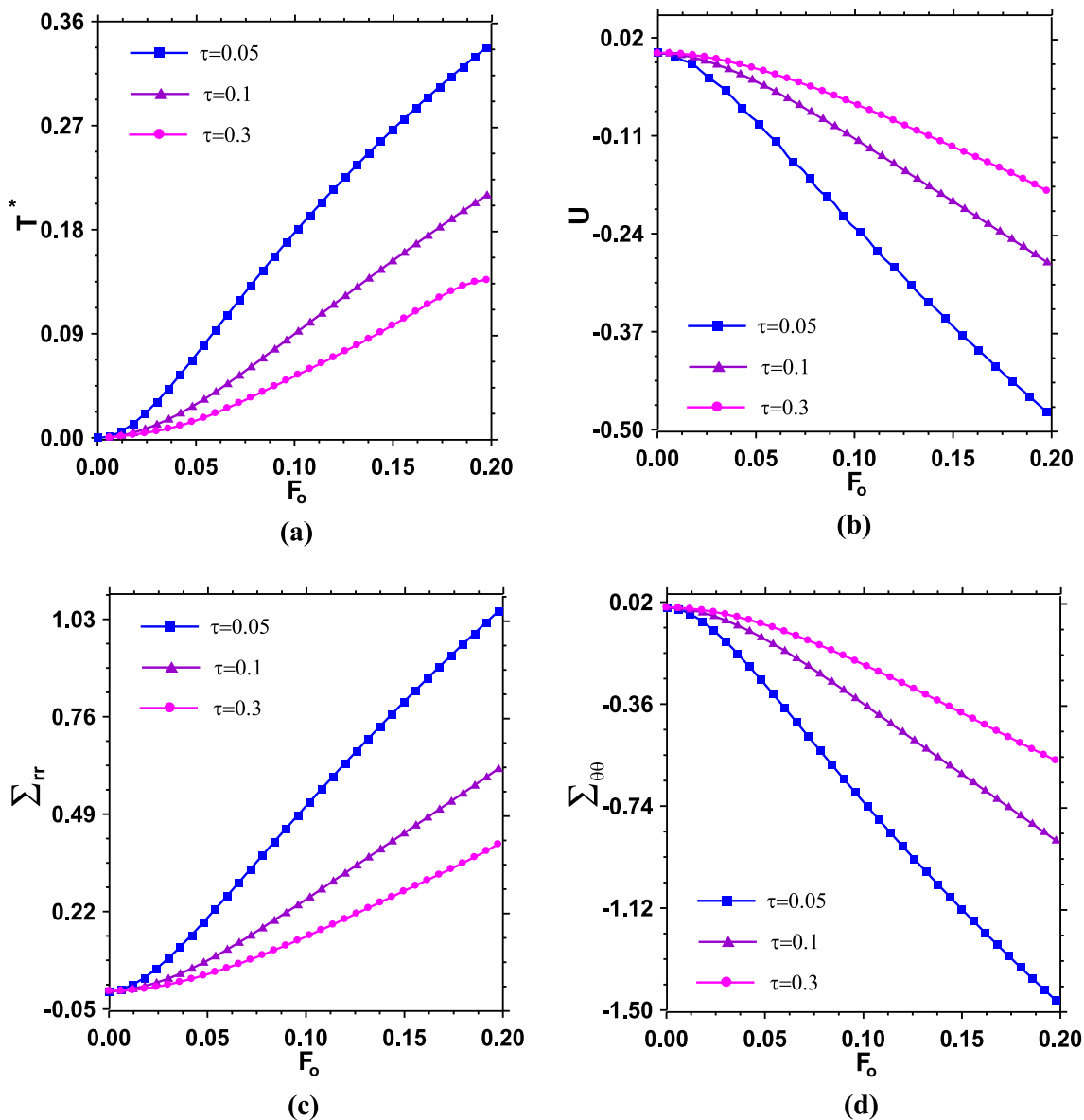


Fig. 12 a–d The influence of relaxation time on the time histories of the results for the spherical shells of type II ($p = 1, \xi = 0.25, \lambda = 0.1$)

The layerwise-differential quadrature method in conjunction with Newmark’s time integration scheme was employed to discretize the governing equations in the spatial and temporal domains, respectively. Then, the

resulting nonlinear system of algebraic equations was solved using the Newton–Raphson method. At first, the fast rate of convergence and accuracy of the method were demonstrated. Then, parametric studies were conducted to

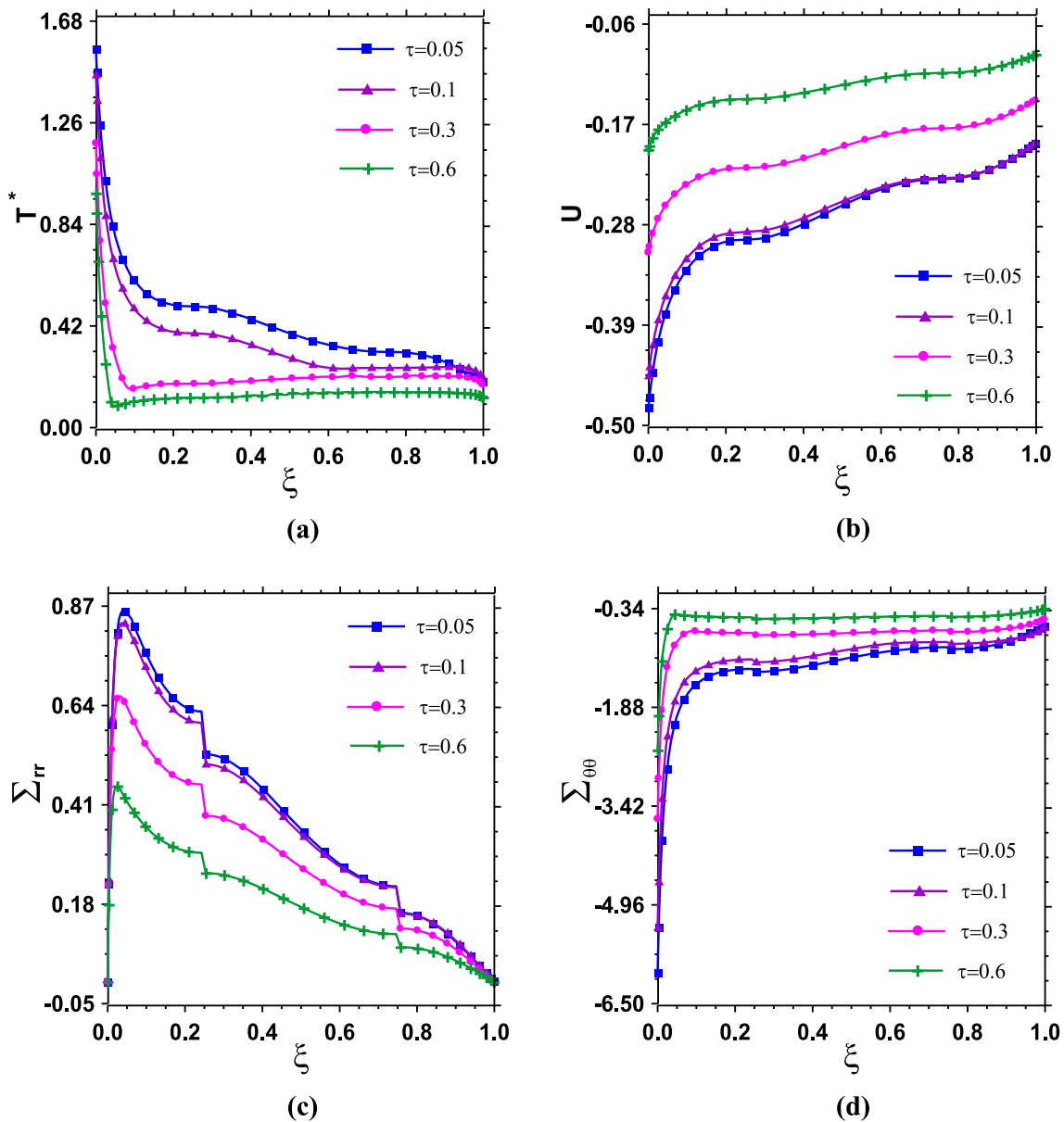


Fig. 13 a–d The effect of relaxation time on the distribution of the results through the radial direction for the spherical shells of type II ($F_o = 0.3, p = 1, \lambda = 0.05$)

illustrate the effects of different parameters on the transient thermoelastic responses of the FG spherical shells and the results were discussed. Through the comparison studies, it was illustrated that the method can accurately predict the thermal wave propagation in the spherical shells. It was shown that the temperature dependence of material prop-

erties, thermo-mechanical coupling, FG layer layout, material gradient index and thickness-to-outer radius ratio have significant effect on the thermo-mechanical behavior of the FG shells. For example, it was shown that by considering the temperature dependence of material properties, all of the non-dimensional thermo-mechanical field vari-

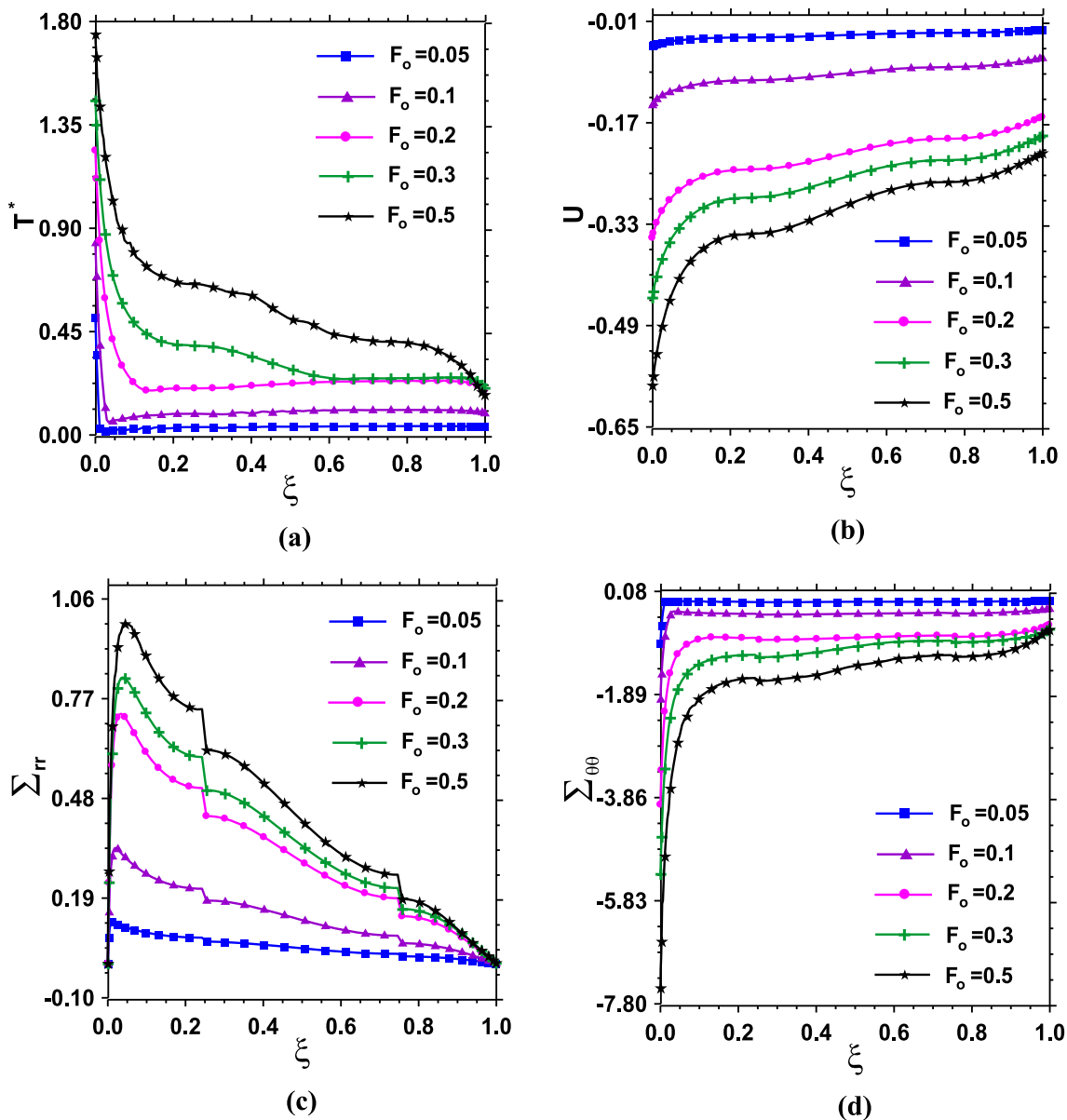


Fig. 14 a–d The effects of different time levels on the distribution of the results through the radial direction for the spherical shells of type II ($p = 1, \tau = 0.1, \lambda = 0.05$)

ables increase. Also, it was found that the propagation of thermal wave for spherical shell made of metal was clearer than those of shells with ceramic and FG materials. Moreover, it was shown that the uncoupled thermoelas-

ticity overpredicts the non-dimensional temperature and radial displacement component of the shell. On the other hand, except the radial stress component, all the other field variables decrease by increasing the thickness-to-outer

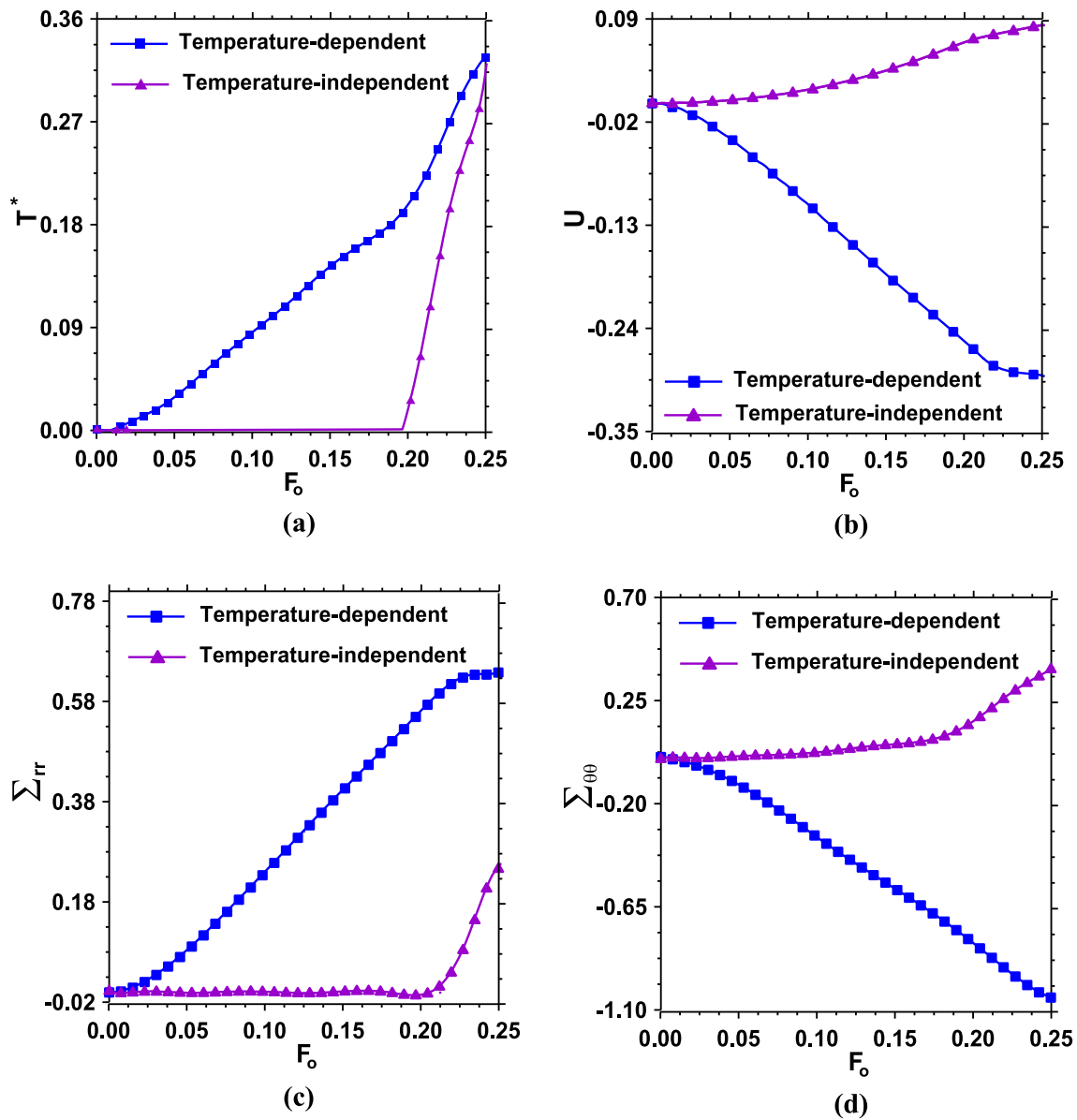


Fig. 15 a–d Temperature dependence of material properties on the time histories of the results for the spherical shells of type II ($p = 1, \tau = 0.1, \lambda = 0.05$)

radius ratio. Furthermore, from the presented results, it was observed that in all cases there were considerable differences between the responses of the homogeneous and non-homogenous spherical shells. And among the different

types of shells under investigation in this study, it was established that the sandwich shells with metal core (i.e., type II) have better thermo-mechanical performance than other ones. For this type of shells (i.e., type II), it was

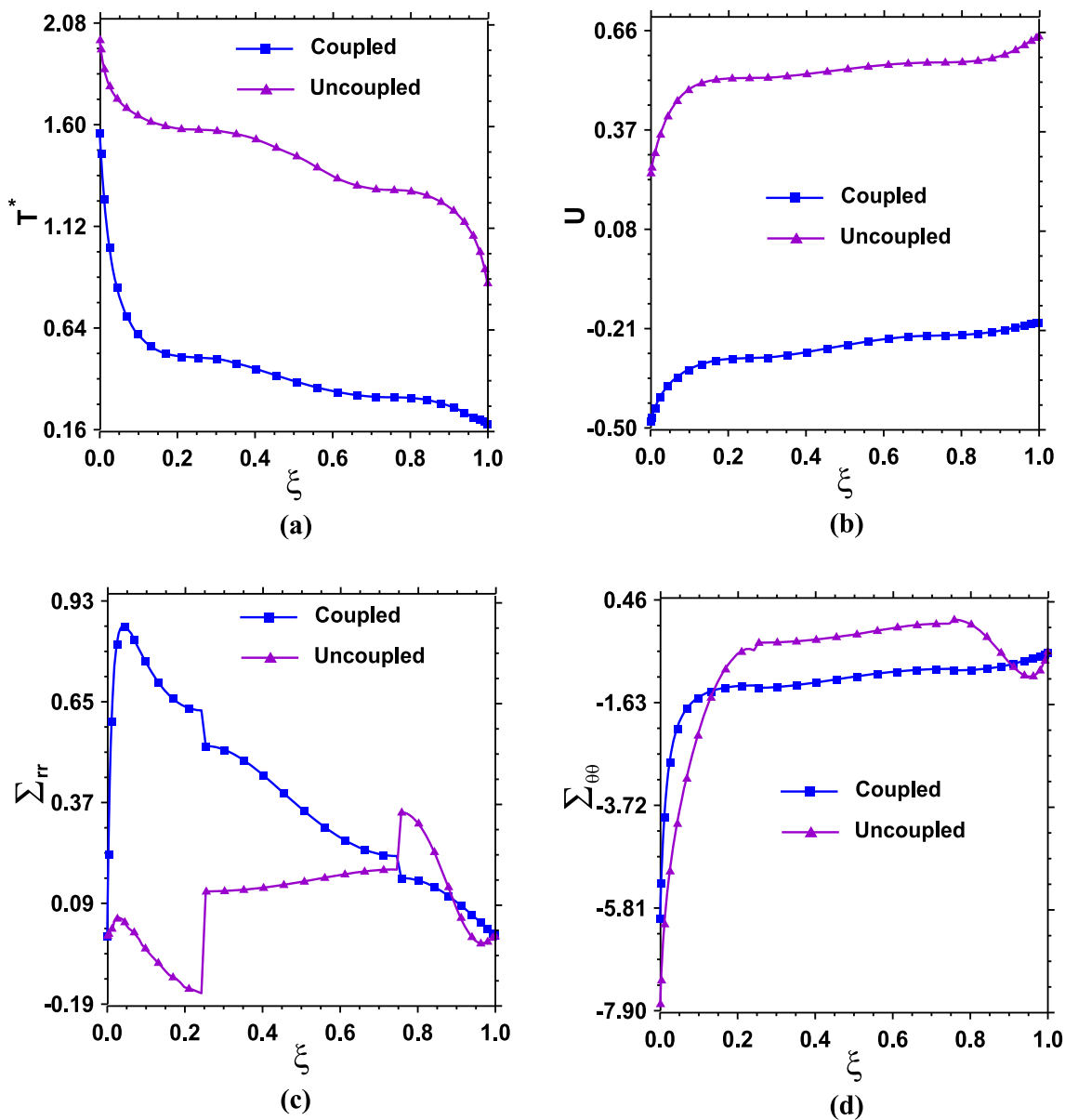


Fig. 16 a–d Comparison of the results for the spherical shells of type II with two different coupled and uncoupled theories ($F_o = 0.3$, $p = 1$, $\tau = 0.05$, $\lambda = 0.05$)

found that by increasing the thickness-to-outer radius ratio, in spite of the radial stress component, all the other field variables decrease. Also, it was seen that by increasing the relaxation time, the non-dimensional temperature, radial

displacement and stress components decrease. However, the relaxation time does not have a significant effect on the variation patterns of these parameters.

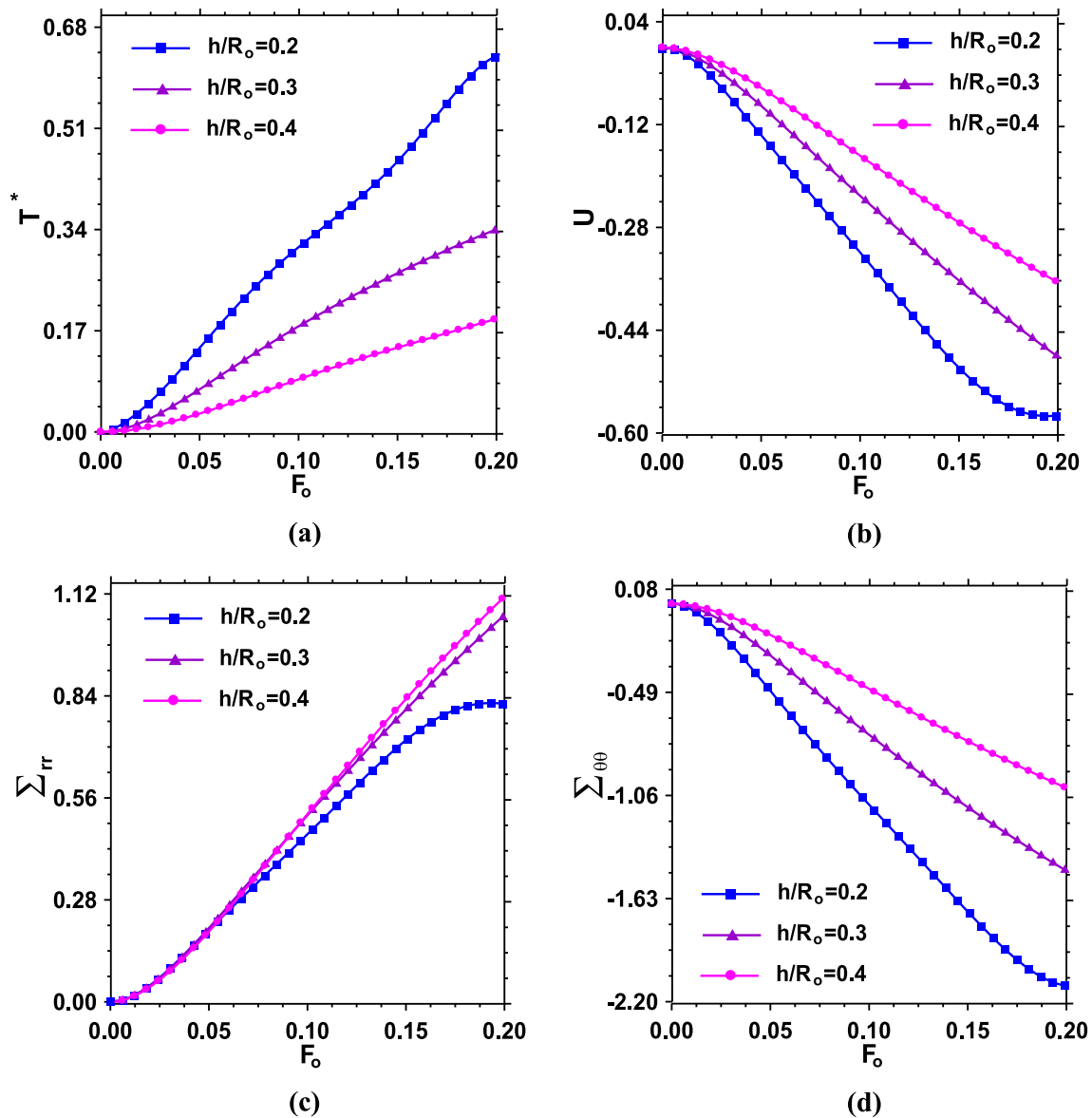


Fig. 17 a–d Time histories of the results against the thickness-to-out radius ratio for the spherical shells of type II ($p = 1$, $\tau = 0.1$, $\zeta = 0.25$, $\lambda = 0.1$)

References

- Akbarzadeh AH, Chen ZT (2014) Dual phase lag heat conduction in functionally graded hollow spheres. *Int J Appl Mech* 6:145002–1–145002-27
- Alavi F, Karimi D, Bagri A (2008) An investigation on thermoelastic behaviour of functionally graded thick spherical vessels under combined thermal and mechanical loads. *J Achieve Mater Manuf Eng* 31:422–428
- Bagri A, Eslami MR (2007) Analysis of thermoelastic waves in functionally graded hollow spheres based on the Green–Lindsay theory. *J Therm Stresses* 30:1175–1193
- Baltacıoglu AK, Akgoz B, Civalek O (2010) Nonlinear static response of laminated composite plates by discrete singular convolution method. *Compos Struct* 93:153–161
- Banic D, Bacciocchi M, Tornabene F, Ferreira AJM (2017) Influence of winkler-pasternak foundation on the vibrational behavior of plates and shells reinforced by agglomerated carbon nanotubes. *Appl Sci* 7(1228):1–55
- Bayat Y, Ghannad M, Torabi H (2012) Analytical and numerical analysis for the FGM thick sphere under combined pressure and temperature loading. *Arch Appl Mech* 82:229–242
- Ching H, Yen S (2006) Transient thermoelastic deformations of 2-D functionally graded beams under nonuniformly convective heat supply. *Compos Struct* 73:381–393

- Chouduri SKR (2007) On a thermoelastic three-phase-lag model. *J Therm Stresses* 30:231–238
- Civalek O (2004) Application of differential quadrature (DQ) and harmonic differential quadrature (HDQ) for buckling analysis of thin isotropic plates and elastic columns. *Eng Struct* 26:171–186
- Civalek O (2006) The determination of frequencies of laminated conical shells via the discrete singular convolution method. *J Mech Mater Struct* 1:163–182
- Civalek O, Korkmaz A, Demir C (2010) Discrete singular convolution approach for buckling analysis of rectangular Kirchhoff plates subjected to compressive loads on two-opposite edges. *Adv Eng Softw* 41:557–560
- Dai HL, Rao YN (2014) Vibration and transient response of a FGM hollow cylinder. *Mech Adv Mater Struct* 21:468–476
- Dai HL, Yang L, Zheng HY (2011) Magneto-thermoelastic analysis of functionally graded hollow spherical structures under thermal and mechanical loads. *Solid State Sci* 13:372–378
- Eslami MR, Babaei MH, Poultangari R (2005) Thermal and mechanical stresses in a functionally graded thick sphere. *Int J Pres Ves Pip* 82:522–527
- Fantuzzi N, Tornabene F, Baccocchi M, Dimitri R (2017) Free vibration analysis of arbitrarily shaped Functionally Graded Carbon Nanotube-reinforced plates. *Compos Part B-Eng* 115:384–408
- Ghosh MK, Kanoria M (2008) Generalized thermoelastic functionally graded spherically isotropic solid containing a spherical cavity under thermal shock. *Appl Math Mech* 29:263–278
- Ghosh MK, Kanoria M (2009) Analysis of thermoelastic response in a functionally graded spherically isotropic hollow sphere based on Green-Lindsay theory. *Acta Mech* 207:51–67
- Gürses M, Civalek O, Korkmaz A, Ersoy H (2009) Free vibration analysis of symmetric laminated skew plates by discrete singular convolution technique based on first-order shear deformation theory. *Int J Numer Meth Eng* 79:290–313
- Hetnarski RB, Ignaczak J (1999) Generalized thermoelasticity. *J Therm Stresses* 22:451–476
- Heydarpour Y, Aghdam MM (2016a) A novel hybrid Bézier based multi-step and differential quadrature method for analysis of rotating FG conical shells under thermal shock. *Compos Part B-Eng* 97:120–140
- Heydarpour Y, Aghdam MM (2016b) Transient analysis of rotating functionally graded truncated conical shells based on the Lord-Shulman model. *Thin Wall Struct* 104:168–184
- Heydarpour Y, Malekzadeh P, Golbahar Haghighi MR, Vaghefi M (2012) Thermoelastic analysis of rotating laminated functionally graded cylindrical shells using layerwise differential quadrature method. *Acta Mech* 223:81–93
- Heydarpour Y, Malekzadeh P, Aghdam MM (2014) Free vibration of functionally graded truncated conical shells under internal pressure. *Meccanica* 49:267–282
- Kiani Y, Eslami MR (2016) The GDQ approach to thermally nonlinear generalized thermoelasticity of a hollow sphere. *Int J Mech Sci* 118:195–204
- Lord HW, Shulman Y (1967) A generalized dynamical theory of thermoelasticity. *J Mech Phys Solids* 15:299–309
- Malekzadeh P, Heydarpour Y (2012) Response of functionally graded cylindrical shells under moving thermo-mechanical loads. *Thin Wall Struct* 58:51–66
- Malekzadeh P, Heydarpour Y (2013) Free vibration analysis of rotating functionally graded truncated conical shells. *Compos Struct* 97:176–188
- Malekzadeh P, Setoodeh AR, Barmshouri E (2008) A hybrid layerwise and differential quadrature method for in-plane free vibration of laminated thick circular arches. *J Sound Vib* 315:212–225
- Malekzadeh P, Golbahar Haghighi MR, Heydarpour Y (2012) Heat transfer analysis of functionally graded hollow cylinders subjected to an axisymmetric moving boundary heat flux. *Numer Heat Tr A-Appl* 61:614–632
- Malekzadeh P, Monfared Maharloei H, Vosoughi AR (2014) A three-dimensional layerwise-differential quadrature free vibration of thick skew laminated composite plates. *Mech Adv Mater Struct* 21:792–801
- Obata Y, Noda N (1994) Steady thermal stresses in a hollow circular cylinder and a hollow sphere of a functionally gradient material. *J Therm Stresses* 17:471–487
- Ootao Y (2009) Transient thermoelastic and piezothermoelastic problems of functionally graded materials. *J Therm Stresses* 32:656–697
- Ootao Y, Tanigawa Y (2004) Transient thermoelastic problem of functionally graded thick strip due to nonuniform heat supply. *Compos Struct* 63:139–146
- Peng XL, Li XF (2010) Thermal stress in rotating functionally graded hollow circular disks. *Compos Struct* 92:1896–1904
- Poultangari R, Jabbari M, Eslami MR (2008) Functionally graded hollow spheres under non-axisymmetric thermo-mechanical loads. *Int J Pres Ves Pip* 85:295–305
- Reddy JN (2006) An introduction to the finite element method, 3rd edn. McGraw-Hill Higher Education, New York
- Santos H, Mota Soares CM, Mota Soares CA, Reddy JN (2008) A semi-analytical finite element model for the analysis of cylindrical shells made of functionally graded materials under thermal shock. *Compos Struct* 86:10–21
- Shao Z (2005) Mechanical and thermal stresses of a functionally graded circular hollow cylinder with finite length. *Int J Pres Ves Pip* 82:155–163
- Shao Z, Wang T (2006) Three-dimensional solutions for the stress fields in functionally graded cylindrical panel with finite length and subjected to thermal/mechanical loads. *Int J Solids Struct* 43:3856–3874
- Sharma PK, Mishra KC (2017) Analysis of thermoelastic response in functionally graded hollow sphere without load. *J Therm Stresses* 40:185–197
- Shen HS (2009) Functionally graded materials: nonlinear analysis of plates and shells. CRC Press, Boca Raton
- Talebitooti M (2013) Three-dimensional free vibration analysis of rotating laminated conical shells: layerwise differential quadrature (LW-DQ) method. *Arch Appl Mech* 83:765–781
- Tornabene F (2009) Free vibration analysis of functionally graded conical, cylindrical shell and annular plate structures with a four-parameter power-law distribution. *Comput Method Appl M* 198:2911–2935
- Tornabene F (2016) General higher-order layer-wise theory for free vibrations of doubly-curved laminated composite shells and panels. *Mech Adv Mater Struct* 23:1046–1067
- Tornabene F, Viola E (2013) Static analysis of functionally graded doubly-curved shells and panels of revolution. *Meccanica* 48:901–930
- Tornabene F, Fantuzzi N, Ubertini F, Viola E (2015) Strong formulation finite element method based on differential quadrature: a survey. *Appl Mech Rev* 67:020801–020801–020801–020855
- Tornabene F, Brischetto S, Fantuzzi N, Baccocchi M (2016a) Boundary conditions in 2D numerical and 3D exact models for cylindrical bending analysis of functionally graded structures. *Shock Vib* 63:1–17
- Tornabene F, Fantuzzi N, Viola E (2016b) Inter-laminar stress recovery procedure for doubly-curved, singly-curved, revolution shells with variable radii of curvature and plates using generalized higher-order theories and the local GDQ method. *Mech Adv Mater Struct* 23:1019–1045

- Tornabene F, Fantuzzi N, Baccocchi M (2017) Linear static response of nanocomposite plates and shells reinforced by agglomerated carbon nanotubes. *Compos Part B-Eng* 115:449–476
- Xiang Y, Ma YF, Kitiornchai S, Lim CW, Lau CWH (2002) Exact solutions for vibration of cylindrical shells with intermediate ring supports. *Int J Mech Sci* 44:1907–1924
- Zenkour AM, Sobhy M (2013) Dynamic bending response of thermoelastic functionally graded plates resting on elastic foundations. *Aerosp Sci Technol* 29:7–17